CARDIFF UNIVERSITY
PRIFYSGOL CAERDYDD

ORCA – Online Research @ Cardiff

This is an Open Access document downloaded from ORCA, Cardiff University's institutional repository:https://orca.cardiff.ac.uk/id/eprint/106178/

This is the author's version of a work that was submitted to / accepted for publication.

Citation for final published version:

Blenkinsop, Thomas , Tripp, Gerard and Gillen, Dave 2017. The relationship between mineralization and tectonics at the Kainantu gold-copper deposit, Papua New Guinea. Geological Society, London, Special Publications , 453. 10.1144/SP453.11

Publishers page: http://dx.doi.org/10.1144/SP453.11

Please note:
Changes made as a result of publishing processes such as copy-editing, formatting and page numbers may not be reflected in this version. For the definitive version of this publication, please refer to the published source. You are advised to consult the publisher's version if you wish to cite this paper.

This version is being made available in accordance with publisher policies. See http://orca.cf.ac.uk/policies.html for usage policies. Copyright and moral rights for publications made available in ORCA are retained by the copyright holders.

The relation between mineralization and tectonics at the Kainantu gold-copper deposit, Papua New Guinea

Tom Blenkinsop[1*], Gerard Tripp[2], Dave Gillen[3]

1. School of Earth and Ocean Science, Cardiff University, Main Building, Park Place, Cardiff CF10 3AT, UK
2. Consulting Geologist, PO Box 42, Woodvale, Western Australia, 6026
3. School of Earth and Environmental Science, James Cook University, Townsville QLD4811, Australia.

*Correspondence: BlenkinsopT@Cardiff.ac.uk

Number of words 8836 (including references and figure captions)
Abbreviated title: Gold and tectonics, Papua New Guinea

Abstract

Epithermal veins and breccias at the Kainantu gold-copper deposit in Papua New Guinea, host gold mineralization in NW-SE steeply dipping lodes. The lodes are parallel to a pre-mineralization dextral strike-slip shear zone network, which is itself parallel in places to an early greenschist facies cleavage in basement schists. The cleavage, shear zone and veins are all cut by dextral strike-slip faults. High Au grades correlate with areas of obliquity between the shear zone fabrics and the cleavage, and plunge at ~40° southeast in the plane of the lodes - coincident with minor fold axes related to a crenulation cleavage in the basement rocks. This clear structural history shows that gold mineralization was confined to a particular late structural event, but lode geometry was influenced by all previous structures, as well as being displaced by post-mineralization faulting. The north-south shortening recorded through most of the tectonic history can be related to Tertiary convergence along the major plate boundary located ~ 15 km north of the mine. However, mineralization occurred under a different tectonic regime from the current north-south convergence, when there was a change of tectonics between 9 and 6 Ma, possibly related to delamination.

Deformation is essential to the formation of hydrothermal mineral deposits. Typical permeabilities of metamorphic rocks in mid to upper crustal conditions that host such deposits are on the order of 10^{-16} to 10^{-18} m^2 (Manning and Ingebritson 1999). With these values, D'Arcy flow of sufficient volume of fluid to form a gold deposit through intact rocks would require geologically unrealistic times. Therefore deformation-induced permeability is a pre-requisite for formation of such deposits, which is also a major reason why these deposits are strongly controlled by structures such as shear zones, faults and fractures (e.g. Sibson 1987; Poulsen and Robert 1989; Hodgson 1989; Robert et al. 1995; Cox 1999).

Important distinctions among hydrothermal gold deposits concern the timing of mineralization with respect to major deformation events. At one extreme, pre-metamorphic gold deposits may not preserve any record of the relevant deformation, and the mineralised assemblage will be overprinted by deformation and high grade metamorphism (e.g. Tomkins and Grundy 2009). At the other extreme, it has been suggested that much gold mineralization coincides with almost the latest tectonic event (e.g. Tripp and Vearncombe 2004; Dirks et al. 2013; Sanislav et al. 2015). The concepts of deeper-earlier vs. shallower-late mineralization (Phillips and Powell 2009) encapsulate this distinction, which is of fundamental importance for exploration and mining, because different structures are likely to have been mineralised at different times.

In many cases of hydrothermal mineralization, relations between mineralization and deformation are hard to establish since regional deformation sequences are not known in detail. In fact studies of mineralization may give the greatest insight into regional structural history (e.g. Weinberg et al. 2004; Miller et al. 2010). It is also quite difficult and therefore unusual to be able to relate mineralizing deformation to specific plate tectonic displacements, although this is also important for mineral exploration on a regional scale. The vast difference in scale between deposit-scale observations and regional tectonics exacerbates this problem.

The Kainantu gold-copper deposit lies 20 km south of the plate boundary between the Australian and the South Bismarck plates in Papua New Guinea (Fig. 1). This study reports on the deformation and mineralization chronology of the Kainantu mine, based on underground mapping and microstructural analysis. Details of the Cenozoic tectonics of the region have been progressively refined over the last 15 years (e.g. Hill and Raza 1999; Hill

and Hall 2003; Cloos et al. 2005; Schellart et al. 2006; Davies 2012; Holm et al. 2015), providing a rare opportunity to relate a mine-scale deformation chronology to plate-scale tectonics. The aim of the paper is to describe the structural evolution with respect to mineralization, and to show how the deformation sequence can be integrated with the plate tectonic scenario in this favourable circumstance.

2. Regional and Local Setting

The Kainantu gold-copper deposit is located ~140 km NW of the city of Lae in the Eastern Highlands Province of Papua New Guinea (PNG) within the Kainantu mineral district (Fig. 1). Kainantu is one of four major mineral districts hosted within Triassic basement metamorphic rocks and volcano-plutonic sequences of the Middle to Late Miocene Maramuni Arc. The Maramuni Arc is a major sector of the PNG Mobile Belt that includes accretionary wedge deposits related to subduction during the Miocene (Hamilton 1979). The Kainantu deposits are hosted within basement metamorphic rocks ~15 km SW of the Markham Valley, a 300 km x 10 km linear active fluvial-alluvial river system that sits atop the active plate boundary between the Australian and South Bismark plates marked by the Ramu-Markham Fault (Fig. 1; Holm et al. 2015).

Major porphyry Cu-Au mineral deposits of the Maramuni Arc include Frieda River (14.3 M oz Au; 7.5 M tonnes Cu; Highlands Pacific Ltd. 2010), porphyry Cu-Mo at Yanderra (1.4 M oz Au; 2.1 M tonnes Cu; Marengo Mining Ltd. 2015) and the world class Wafi-Golpu deposit (28 M oz Au; 9 M tonnes Cu; 50 M oz Ag; Newcrest Mining Ltd. 2015) (Fig. 1). The Kainantu mine is developed on the Kora-Irumafimpa vein system of quartz-telluride-base metal low-to-intermediate sulphidation veins associated with porphyry copper centres (Fig. 2). The system trends NW with a length of over 2.5 km, and consists of the Kora, Eutompi, Irumafimpa, Judd and Upper Kora veins (Vigar et al. 2015). The Kora-Irumafimpa vein system is itself part of a network of fault-hosted epithermal veins that include Maniape and Arakompa carbonate-base metal veins (Corbett et al. 1994; Corbett and Leach 1998), radially disposed about an interpreted porphyry centre (Fig. 2; Corbett and Leach 1998). Epithermal, crustiform and colloform, quartz-adularia pyrite (low-Fe sphalerite) veins and breccias show a progression to higher sulphidation states (quartz-chalcopyrite +/- bornite-Au) towards the SE,

along the vein lodes, approaching the interpreted porphyry centre, overlain by the high sulphidation (quartz-alunite-pyrite-enargite) lithocap at Bilimoia. The Kora-Irumafimpa vein system has current resources of 1.5 Moz Au, 5 Moz Ag, and 0.1 M tonnes Cu (Vigar et al. 2015).

Detailed paragenetic studies by Espi et al. (2005, 2007) have established a 10 stage history, in which gold was only precipitated in stage 8, in association with Te and Bi, at temperatures below 350°C, due to change in sulphidation and oxidation state, from oxidised magmatic fluids. Later stages include carbonates and a supergene overprint. Low salinity aqueous-carbonic fluid inclusions from stage 4 suggest quartz precipitation at 210-300°C, and fluid immiscibility.

Economic vein mineralisation at Kainantu is hosted within basement greenschist facies schist, gneiss, phyllite, metagreywacke and meta-arkose of the Bena Bena Formation of Middle to late Triassic age (Van Wyck and Williams 2002) that were likely sub-marine flysch sequences (Tingey and Grainger 1976). The Bena Bena Formation at the mine is dominantly phyllitic. The Bena Bena Formation and the Owen Stanley Metamorphics (also predominantly low grade metasedimentary rocks including graphitic slate, and chlorite and sericite schists, and some blueschists: Davies and Smith 1971) are basement to overlying Oligocene to Miocene calcareous greywacke with interbedded siltstone and limestone of the Omaura Formation, and Middle Miocene volcanic rocks of the Yaveufa Formation including basaltic andesitic, and subordinate marine sedimentary rocks. The basement metamorphic rocks were extensively intruded by the Middle Miocene batholithic Akuna diorite-granodiorite, and the Late Miocene Elandora hornblende porphyry suite, with a close association between the latest most fractionated intrusion phases and porphyry associated mineral deposits (Corbett et al. 1994).

3. Data and Methods

This paper is based on 1:250 underground mapping of levels 17 (~ 1400 m above sea level) to 21 (1279 a.s.l.) at Kainantu mine, kinematic and dynamic analysis, and microstructural studies. Underground maps are displayed on the mine grid (also used for underground location descriptions), which is orientated at 321°, but all azimuths are given relative to true

north. Orientated samples of representative structures were collected and thin sections examined in transmitted light microscopy. A younging table (cf. Angelier 1991) was used to determine paragenetic relationships among veins. Faults were analysed by both kinematic and dynamic methods to obtain the principle strains and stresses (cf. Blenkinsop 2006). Linked Bingham distributions of the P and T axes of these faults were used to find the principal strain axes (extension positive) in a kinematic analysis (cf. Marrett and Allmendinger 1990) using FaultKin 4.3 (http://www.geo.cornell.edu/geology/faculty/RWA/RWA.html). The right trihedra method and the inversion method as presented in Ramsay and Lisle (2000) were used to perform dynamic analyses to obtain the principal stress orientations ($\sigma_1 \geq \sigma_2 \geq \sigma_3$, compression positive). and the ratio $\Phi = (\sigma_2 - \sigma_3)/(\sigma_1 - \sigma_3)$, and the average angular deviation between the measured and theoretical slip directions. The kinematic and dynamic analyses allowed the structures to be related to the tectonics of PNG.

3. Description of Structures

3.1 Regional Cleavage S1, L1

S1 is a slaty cleavage in phyllites (Fig. 3a). It is vertical to sub-vertical and trends NW-SE (Fig. 4). The intensity of S1 in phyllites varies from strong (Fig. 3a) to weak although throughout most of the mine it is moderately developed. L1 is a mineral stretching lineation defined by phyllosilicates and visible on the surface of S1. L1 varies from moderate to absent on S1 surfaces, the intensity varying approximately with that of S1. L1 is less well developed in the phyllites than S1, so that they can be referred to as S>L tectonites. L1 is sometimes seen as a faint banding which may be an L^0_1 intersection lineation, although bedding cannot be positively identified.

The orientation of S1 is constant throughout the mine except in two circumstances: S1 is affected by D2 kinks on a metre scale, and in the anomalous area north of 59990N on 19 and 20 levels (Fig. 5). In this area an anticlockwise rotation of 20º in S1, L1 and L^1_2 occurs. Figure 5 shows that the change in orientation occurs in an area adjacent to a shear zone, while foliation in that shear zone (Sm) remains in the general NW-SE orientation. Thus the

structural data show a spread that encompasses both the general NW-SE orientations and anticlockwise-rotated orientations. This change in strike may be significant for gold grades.

3.2 Shear Zones and Mylonites: Sm, Lm

An intense Sm fabric defines a network of mylonites in shear zones that can be mapped throughout the mine. Sm is associated with a sub-horizontal mineral stretching lineation Lm which is a mineral stretching lineation similar to L1. The shear zone boundaries are generally sharply defined by an increase in intensity of the fabric over a few cm at most. The shear zones dip very steeply to the NE or E. A distinctive aspect of the shear zone geometry is a pattern of NW and NNW striking segments (Fig. 5). Thicker (2 – 3 m wide) and longer segments strike NW and are connected by thinner (0.5 – 1m) and shorter NNW-striking segments, creating a network of shear zones around lozenge-shaped lithons. Up to three parallel NW-striking shear zones, approximately 10 m apart, are linked by NNW-striking shear zones at intervals of 20 – 30 m. This distinctive geometry is repeated throughout the southern part of the development. Sm fabrics within and adjacent to the shear zones are parallel to sub-parallel to the shear zone boundaries. At 59750 – 59760 N on 20 level, exposure of the mylonites in the floor of the development drive shows excellent shear sense indicators in the form of SC fabrics and sigma clasts of quartz a few cm in diameter (Fig. 3b). The shear zone network geometry changes north of 59990N. Sm fabrics strike WNW instead of the general NW direction observed to the south. There are corresponding segments of shear zones in this orientation.

3.3 Intersection Lineation, L^1_2, Crenulation Cleavage S2

L^1_2 is a common fabric seen on S1 and Sm surfaces as a crenulation lineation (Fig. 3c). It is referred to as L^1_2 on both S1 and Sm surfaces for simplicity. The planar fabric S2 that causes L^1_2 is only visible in areas of very strong L^1_2, where it can be seen as a surface generally dipping steeply to the E. Generally L^1_2 is moderately developed, but it can become as strong as a strong S1 fabric (Fig. 3c), and it is absent in places. L^1_2 plunges moderately to steeply SE (Fig. 4).

3.4 Kink Bands and Folds

Kink bands on a cm to m scale affect the orientation of S1 and L1 in several places. The axes of the kinks plunge parallel to L^1_2 (Fig. 4). Within the mylonites, on 20 level between 59760 N and 59770 N a quartz-albite vein has isoclinal folds with axes similar to L^1_2 and an axial surface parallel to S2 (Fig. 3d).

3.5 Breccia Veins

The Kora-Irumafimpa vein system underground is mapped as a number of separate veins that contain the mineralised lodes, known as the Mill, Robinson and Puma Lodes, of which the Mill Lode is the most persistent. The lodes are hosted in breccia veins up to several metres wide with distinctive textures. The fragments in the breccias consist of mylonites up to several cm in size, which have been strongly altered to a fine-grained phyllosilicates including fuchsite (Fig. 3e,f). The matrix to the breccias consists of grey, clear or white quartz, commonly having fibrous textures with colloform banding. Open vugs up to several cm in size are lined by prismatically terminating quartz fibres (palisade structure), which are continuous with the matrix quartz. Coarse grained pyrite occurs in the foliated mylonitic clasts and in the quartz veins.

3.6 Faults, Fault zones, Gouges, Slickensides and Slickenlines, Joints

Faults occur as sharp planes on one or both sides of gouge zones filled by grey clay fault gouge. Individual faults have been mapped up to 80 m along strike, and gouge thicknesses may be up to 3 m. Faults are vertical to sub-vertical, with very consistent NW-SE strikes (Fig. 5). Fault planes are commonly slickensides with a shiny graphitic coating. Delicate slickenlines probably formed as scratches can be seen on the slickensides. The vast majority of these are sub-horizontal, but sometimes an overprinting steeply plunging lineation can be seen.

The gouge zones display classic textures for fault gouges: a prominent P-foliation is visible, cut by Riedel shears and anastomosing around asymmetric shear band type boudins (Fig. 3 g, h). Shear sense indicators from P foliations, Riedel shears and asymmetric boudins are all

consistently dextral for all faults examined with one exception. Faults can clearly be seen cutting across the S1, Sm, and S2 fabrics and quartz-pyrite mineralization. A system of vertical north-south joints crosscuts all other features. The largest of these is a mine-scale feature called the Chinook structure.

3.7 Summary

Table 1 summarise the inferred deformation chronology at Kainantu based on cross-cutting and overprinting relationships. There are at least six clearly separate deformation events, which in general record a progression from penetrative, continuous deformation at a metre scale to discontinuous deformation. Many of these features are parallel or sub-parallel, including S1, Sm, breccia veins, and faults. Simple kinematic interpretations suggest that D1, Dm, D4 and D5 are compatible with north-south shortening.

4. Microstructures

The major aims of thin section petrography were to provide details of the structural history and insight into deformation mechanisms. The dominant minerals in all sections were quartz, muscovite, chlorite and pyrite, with subordinate fuchsite/sericite, garnet, titanite, epidote, carbonate and biotite. The microstructures observed can be classified as S0/S1, Sm, S2, and veins. Sample locations are provided in Table 2.

4.1 Description of Microstructures

S1. The earliest fabric visible is banding of quartz and muscovite/chlorite layers 0.2 – 1 mm wide, with a strong alignment of the phyllosilicates. The layering may have originated as S0, but is defined as S1 because no unequivocal bedding could be identified in thin sections. Quartz grains (0.001 to 0.1 mm) generally have equant shapes and straight grain boundaries, with no internal strain features. A scattering of very well aligned muscovite within the quartz layers demonstrates that all minerals have been completely recrystallized from their precursors. The observation that S1 bands in the N section (perpendicular to the lineation) are

lens-shaped compared to the tabular shapes in P sections (parallel to the lineation) suggests that S1 has a component of linear fabric: it may be classified as an S>L tectonite fabric.

Sm. Sm has similar characteristics to S1: a quartz/phyllosilicate banding with a strong grain shape fabric in the phyllosilicates (Fig. 6a). However, a number of features indicate that Sm formed from higher strains than S1. Isoclinal folds of the S1 layering are observed in some sections, and kink bands, undulatory extinction and sutured grain boundaries preserve evidence for dynamic recrystallization by grain boundary migration. Quartz grains may be elongate to define the mylonitic fabric; in sample K10, this quartz grain shape fabric is due to grain boundary pinning between scattered phyllosilicates.

Sample K8 reveals the relationship between S1 and Sm. In this sample Sm is a differentiated crenulation cleavage of muscovite and opaque minerals, in domains 0.05 mm wide spaced at 0.15 – 0.3 mm and axial planar to tight to isoclinal folds of S1 (Fig. 6b). This clear overprinting relationship between S1 and Sm is particularly significant because the sample comes from the northern end of 20 level where S1 fabrics strike WNW instead of the general NW direction observed to the south. The overprinting relationship suggests that S1 is reactivated along most of the lodes to form Sm, but where S1 is oblique to Sm in the northern parts of the mine, S1 is crenulated to form a distinct Sm.

S2. S2 is an asymmetric crenulation cleavage with a distinctly S shaped geometry when viewed from above (Fig. 6c). The cleavage is defined by the long limbs of highly asymmetric folds, and are typically spaced 0.2 - 1 mm apart. These limbs are concentrations of phyllosilicates and opaque minerals. S2 is consistently 12–30º clockwise of Sm in sections perpendicular to the foliation and parallel to the lineations. In some places S2 is defined by discrete kinks in muscovite. S2 clearly overprints Sm.

Fault gouge. Sample K4 of fault gouge is dominated by chlorite in laths up to 0.1 mm long. Quartz grains 0.08 mm in size with undulatory extinction comprise the remainder of the rock except for some green-brown biotite with the same habit as the chlorite.

4.2 Mineral Paragenesis

S0/S1 and Sm are defined in most samples by quartz, muscovite and chlorite. Garnet overgrows S1, but appears to be pre-tectonic with respect to Sm. S2 is defined by the same minerals as Sm, with some opaque mineral mobility, and clearly overprints garnet. Chlorite defines Sm and replaces S1; it also defines the fabric in the fault gouge. Pyrite can be identified as a vein phase in several types of vein (see below). Fuchsite/Sericite is a significant phase only in the Mill and Puma Lode samples, where it appears to define Sm.

4.3 Veins

32 veins were observed in the thin sections. They could be classified into six different types mainly based on the type of vein fill. These distinctions are not necessarily significant in every case because not all filling components may be visible in the section. Nevertheless, some clear distinctions and age relationships are visible.

Vq. Quartz only veins 0.1 to 3 mm wide, with irregular or sharp margins. Blocky or fibrous quartz in optical continuity with host rock quartz grains widens towards centre of vein, implying syntaxial growth (Fig. 6d). Abundant small inclusion trails are parallel to fibres. Although veins cut Sm, they are also folded with Sm (implying emplacement syntectonically with mylonitisation). Vein fills may change along strike from fibrous, where perpendicular to Sm, to recrystallized where parallel to Sm, and they may become segmented. These veins may be isoclinally folded with Sm axial planar.

Vqp. Quartz-pyrite ± titanite veins 0.1 – 1.0 mm wide with sharp margins. Quartz-pyrite veins can change from 100% quartz to 100% pyrite along their length (Fig. 6e). Fillings may be blocky or fibrous, widening towards the centre of the vein indicating syntaxial growth. Primary fluid inclusions outlining prismatic quartz shapes are visible in some places. There may be abundant fluid inclusion planes. Inclusion bands of pyrite may occur parallel to vein margins. The veins are planar when parallel to S0 and folded when cutting S0. These veins may be continuous with similar fillings in vugs. Like Vq veins, they cut Sm and are folded with Sm

Vqc. Quartz-chlorite ± carbonate, epidote, titanite, pyrite, plagioclase veins 0.1- 0.4 mm wide, with sharp or indistinct margins, filling of fine-grained aggregates of various minerals. These veins cuts S1 and Sm, but are deformed by Sm.

Vsp. Fuchsite/Sericite-quartz veins 0.1 - 0.3 mm wide, with planar margins and profiles. A core of euhedral opaques has a sericite margin.

Vc. A chlorite vein 0.8 mm wide with sharp but irregular margins and folded shape. Chlorite fibres are parallel to Sm. This vein cuts Sm but is folded with Sm.

Vt. Titanite veins 0.01-0.02 mm wide with sharp margins and planar shapes. The veins have a filling of very fine-grained titanite, and are parallel to Sm.

4.4 Vein Paragenesis

All veins can be inferred to postdate S1 and Sm, except the Vq veins which may be partly contemporary with Sm. Several other cross cutting relationships observed in the thin sections are summarised in the younging table (Fig. 7), which clarifies that there are several possible histories permitted by the thin section constraints. The younging table indicates a preferred chronology: Sm→Vq→S2→Vqp→Vqc→Vsp→Vc→Vt. However, thin sections observations allow several permutations: for example, S2 and Vsp may occur anytime in the chronology after Vq, Vqc anytime after Sm, and Vc, Vt anytime after Vqp.

4.5 Microstructural History

Figure 8 integrates the microstructural history, mineral and vein paragenesis with the structural history. A critical point established from the microstructural studies is the separation between the regional deformation producing the early S1 fabric and the subsequent mylonitisation. This is most clearly exemplified by the observation that Sm is a crenulation cleavage. The microstructural observations also establish that S2 clearly overprints Sm and is a separate event, unrelated to any significant veining or sulphide precipitation. The earliest veins (Vq) may have been contemporary with mylonitisation, but subsequent veins appear to accompany brecciation along the lodes.

In summary, the microstructural record complements and supplements the underground observations and has lead to important refinements of the geological history. The major conclusion is that a record of at least six distinct events is preserved, and that mineralisation is controlled by reactivation of earlier structures in specific events.

5. Fault Slip Analysis

Figure 9 shows the orientations of all 76 faults measured (Fig. 9a) and the kinematic and dynamics analyses carried out on 14 faults with confirmed sense of shear for kinematic analysis, and 34 faults with slickenlines for inversion (Fig. 9b-e). The kinematic analysis shows north-south shortening during faulting (Fig. 9c). Both methods of dynamic analysis show north-south σ_1 (Fig. 9d,e). The inversion additionally shows a strike-slip stress system with a subvertical intermediate principal stress (Fig. 9e) and gives a stress ratio Φ, $(\sigma_2 - \sigma_3)/(\sigma_1 - \sigma_3)$, of 0.3 with a deviation of 24°. This is a globally common value for Φ (Lisle et al. 2006), and the deviation is also a fairly typical result for this type of inversion.

The kinematic and dynamic analyses for the post-mineralization faults suggest north-south shortening and east-west extension, in a strike-slip stress regime. These kinematics are similar to those inferred for the dextral strike slip shear zones in Dm. This suggests that the structural history visible at Kainantu has involved at least two episodes of north-south shortening, pre and post mineralization respectively.

6. Discussion

6.1 Structural Controls on mineralization

It is evident that the entire structural history has influenced the present disposition of the ore at Kainantu mine. The shear zone network, in which the mylonitic fabric Sm was formed, is largely parallel to S1 (Figs. 4, 5). Both S1 and Sm were affected by crenulations during D2,

with crenulation hinges plunging to the southeast (Fig. 4). The shear zones have distinctive right–hand bends, so that they consist of long NW trending segments joined by shorter WNW segments. The breccia veins are mainly parallel to the mylonitic shear zone network (Fig. 5). The gold-copper mineralization, which postdates the main veins of pyrite-quartz breccia, is localised within these veins, although it is difficult to observe a specific structure underground that corresponds to this mineralization. A variety of other vein types occur with the pyrite-quartz breccia, but it is not clear which, if any, are specifically associated with gold mineralization. This situation illustrates an important point about hydrothermal gold mineralization: veins that are parallel to mineralised lodes should not axiomatically be linked to mineralization, especially where their orientation is influenced by pre-existing structures. Finally, faults that cross-cut all previous structures are also largely guided by the shear zones, and offset the ore-bearing lodes.

In long section, there is a SE plunge to the mineralization (Fig. 10) that corresponds to both bends in the shear zone network and S2 crenulations. Notably higher grade mineralization occurs where veins are oblique to the S1 foliation. There is a striking correlation between the high grades at the northern end of 20 level and an obliquity of about 30º between the two fabrics (Fig. 5). Where the fabrics are parallel, in the southern part of the drive, there is less brecciation and lower grades, except for the far southern end of the drive, where Sm also changes by becoming weaker.

6.2 Miocene-Recent Tectonic History of NE Papua New Guinea

The highlands of Papua New Guinea have been affected throughout the Cenozoic by north-south convergence as the Australian craton has moved northwards. Details of this process can be complex, involving terrane accretion, transcurrent movement and rotation (e.g. Klootwijck et al. 2003a). Figure 11 shows some of the more recent scenarios reported in the literature.

In an extensive synthesis of mid-Miocene to recent plate movements along the northern Papua New Guinea margin, Hill and Raza (1999) divide the time from 18 Ma to present into three tectonic phases, based largely on constraints from fission track chronology:

1) 18-12 Ma. A S-dipping subduction zone off the coast of NE Papua New Guinea subducts the Solomon Sea plate with a westerly movement direction. However, NE Papua New Guinea is in a state of NE-SW extension in the back arc.
2) 12 – 4 Ma. Continued oblique subduction. However there is a major change to back arc compression, uplift and denudation in NE Papua New Guinea.
3) 4 Ma – Present. Rapid convergence of the Finisterre Terrane and transpression. Overall more oblique convergence than in the previous phase (Wieler and Coe 2000). Older papers, e.g. Cullen (1996), Crowhurst et al. (1996), suggest Finisterre collision from 10 Ma.

By contrast, the large scale reconstruction of Schellart et al. (2006) suggests the following tectonic history, based on a model that emphasises the importance of roll-back at subduction zones, which generates extensional stresses in the overriding plate. This model is constrained by relative plate motion data.

1) 40 – 30 Ma: North-dipping subduction. Roll-back in a southerly direction brings the New Guinea arc into collision with the New Guinea passive margin at~ 30 Ma. Arc collision at this time would involve a component of north-south shortening.
2) 30 – 15 Ma: South-dipping subduction along the Australian – Pacific plate boundary continues.
3) 15 – 5 Ma: A new south-dipping subduction zone, the Trobriand trough, initiates immediately to the North of the Papua New Guinea coast in response to the collision of the Ontong-Java plateau. This trench rolls back to the north, possibly allowing for north-south extension in Papua New Guinea.
4) 5 – 0 Ma: Roll-back of the New Britain trench opens the Manus basin. Replacement of the Trobriand trough by the New Britain plate boundary on Papua New Guinea.

A more recent account of the tectonics of this region by Holm et al. (2015) focuses on the Maramuni arc, on the basis of new geochronology and geochemistry of intrusive rocks. The Maramuni arc is defined as “all Late Cenozoic magmatism with a subduction-related geochemical signature” which occurs throughout the Papuan fold and Thrust belt.

1) Prior to 12 Ma, northward subduction of the Pocklington Sea slab occurred at the Pocklington trough, leading to collision of the Australian continent and initial growth

of the New Guinea orogeny. Foliated tonalities at Wamum (Fig. 1) are associated with this subduction phase.

2) By 9 Ma, northward subduction of the Solomon Sea plate beneath the Finisterre terrane was occurring at the New Britain trench. Tonalites intruded near Kainantu (Kokofimpa tonalities) have ages of 9.4 - 8.7 Ma, and show increased evidence for crustal components.
3) At 6 Ma, lithospheric delamination of the Pocklington sea slab occurred, resulting in magmatism and renewed orogenesis in the New Guinea orogeny. The porphyritic dacites intruded in this phase may have been the source of fluids and metals for mineralization.
4) At 3 Ma, the Solomon Sea has closed and the Finisterre Terrane is thrust onto the New Guinea Mobile belt: convergence continues today along the Ramu-Markham fault.

For the 15-5 Ma period Hill and Raza (1999) and Holm et al. (2015) imply compression in the Kainantu area, while Schellart et al. (2006) imply extension. The Schellart et al. (2006) model is also distinct from the other two in implying a south-dipping subduction zone. However, all models agree on a major change between 9 and 6 Ma at which time slab break-off (Holm et al. 2015) or rollback (Schellart et al. 2006) may have lead to a period of extension, coincident with the 7-9 Ma age of Elandora Porphyry intrusions and associated mineral deposits (Griffin 1979). The major differences between the scenarios are the presence/absence of a south dipping subduction zone to the North of PNG, and its role in magmatism. Holm et al. (2015) argue that the magmatic history is more consistent with control by northward dipping subduction. These large-scale kinematic constraints may translate to complex kinematics on a small scale (Klootwijk et al. 2003b).

6.3 Contemporary Tectonics

Today, the Ramu valley and the Ramu-Markham fault mark the junction between the South Bismarck and the northern margin of the Australian plate (which may be referred to as the New Guinea Highlands microplate), and their relative motion can be described by a clockwise rotation of the South Bismarck microplate about an Euler pole at approximately 144º E, 5º S (Wallace et al. 2005). This rotation has been occurring since the initiation of Finisterre collision at 3.5 – 4 Ma (Abott et al. 1994; Weiler and Coe 2000). Convergence due to this

477 rotation is expressed seismically by a northward-dipping zone of foci, with reverse fault focal
478 mechanisms (Pegler and Woodhouse 1995). Figure 12 shows the present day strain rates from
479 the ILP Global Strain rate map (Kreemer et al. 2003) relative to Australia. The NE
480 convergence of the whole of NE Papua New Guinea relative to Australia is clear, as is the
481 significant zone of high strain rates within and to the north of Papua New Guinea.
482
483 The present day stress field of the same area is shown in Fig. 13. Although there are relatively
484 few measurements from onshore Papua New Guinea, they are generally consistent with NS to
485 NNE-SSW compression or strike-slip, and thus with the dynamic and kinematic analysis
486 shown in Fig. 9 for the late strike slip faults.
487

488 ### *6.4 Tectonics and Mineralization at Kainantu Gold-Copper Deposit*

489 Several results of this study can be integrated well with the tectonic history described above.
490 The kinematic and dynamic analysis of the D5 faults indicated north-south shortening with a
491 north-south maximum principal stress (Fig. 8). This is compatible with the present day plate
492 motions and stress field orientation (Figs. 12, 13), which are likely to have been in place for
493 the last 4 – 5 Ma. Stress inversion suggests a strike-slip fault regime in which σ_2 is vertical,
494 but most of the in situ stresses suggest a thrust fault regime. This is a logical and likely
495 consequence of exhumation from the time of faulting, since the vertical principal stress will
496 decrease as erosion occurs. The north-south orientation of σ_1 would lead to dextral resolved
497 shear stress on NW trending faults, as observed. The north-south joint system, including the
498 Chinook structure, developed in this stress regime and its orientation is broadly compatible
499 with this stress field.
500
501 Mineralisation apparently involved dilation of the lodes, implying a different stress regime
502 from the present day and from most recent, strike slip faulting. The extensional vein nature of
503 much of the quartz within the lodes suggests that mineralisation was not related to dextral
504 strike–slip deformation. Instead, it is convincingly associated with the change in tectonics
505 between 9 and 6 Ma by the ages of the later intrusive rocks at Kainantu (Holm et al. 2015).
506 Extension related to the roll-back of the Trobriand trough subduction zone (Schellart et al.,
507 2006) is one possibility for causing this change, and the delamination advocated by Cloos et
508 al. (2005) and Holm et al. (2015) is another. This tectonic phase is clearly separate from the
509 current convergent phase, and the preceding phase of convergence.

The kinematics of S2 are poorly understood but may have involved E-W shortening and NS extension; this could also be compatible with roll-back. The preceding deformation during mylonitisation suggests a prior episode of north-south shortening in a strike-slip regime. This would be compatible with collision of the New Guinea arc at 30 – 40 Ma, or with the convergence suggested by Hill and Raza (1999) and Holm et al. (2015) for the period from 12 to 9 Ma. The timing of S1 is unconstrained by observations in this study, but the Bena Bena Formation may have been deformed in the Jurassic (Page 1976), so that S1 may considerably predate the Neogene events described above, even though it may have influenced subsequent deformation.

Therefore the three major tectonic phases in the Late Miocene to recent history of NE Papua New Guinea are reflected in the structures at Kainantu mine, and gold-copper mineralization can be related to the middle phase, corresponding to roll-back or delamination. The scenario of a delaminated, stalled slab has been identified by Sillitoe (1997) as one of the ingredients in large porphyry and epithermal deposits in the circum-Pacific region: partial melting of such slabs may cause oxidation of the upper mantle and release of gold. In more detail, it is possible that the Kora-Irumafimpa vein system records early events in the second phase in the form of the coarse pyrite and breccia lodes (Espi et al. 2007; Vigar et al. 2015), while the later stages are represented by gold and copper mineralization within these lodes (Stage 8 of Espi et al. 2005). That the mine-scale deformation can be related to plate tectonics in this study is due to a favourable combination of recent mineralization which is hardly overprinted, proximity to a plate boundary, and detailed knowledge of the plate tectonic situation.

7. Conclusions

1. Six deformation events can be recognised at Kainantu Mine.
    - The first deformation was the production of a NW trending subvertical regional cleavage (S1) under greenschist facies conditions.
    - This was followed by the development of mylonites with foliation Sm in a NW-trending shear zone network which reactivated S1 except where S1 was oblique to Sm in the northern part of the mine, where S1 was crenulated. The mylonitic shear zones

543 have dextral strike-slip kinematics and a distinctive pattern of longer and thicker NW-
544 striking segments joined by narrower and shorter NNW-striking segments.
545 • S1 and Sm were overprinted by asymmetric crenulation cleavages in S2: the dominant
546 visible effect was the production of a moderately SE plunging intersection lineation.
547 • Zones of brecciation developed on the shear zone network next, with the major gold
548 mineralising event being localised within the breccias.
549 • NW dextral faulting within and along the shear zone network then effected minor
550 displacements of the breccia veins.
551 • North-South sub-vertical joints were formed as the most recent event.
552
553 2. Reactivation of earlier fabrics is a critical process at Kainantu. The shear zone network
554 followed the earlier regional cleavage (S1), and the breccia veins followed the shear zone
555 network. Gold mineralization occurred within the breccia veins. The unusually planar nature
556 of the shear zones is due to control by the earlier S1 fabric, which generally has a consistent
557 NW-trending, sub-vertical orientation. Where the mylonitic foliation Sm is oblique to S1,
558 gold grades appear to be enhanced. Such repeated reactivation, by parallel structures many of
559 which were unconnected with mineralization, could obscure true structural controls on
560 mineralization and their relationship to tectonic events in other situations; however the
561 relatively recent and well-preserved history at Kainantu have allowed the history of
562 reactivation to be deciphered.
563
564 3. There are clear relationships between the regional plate tectonic history and the structural
565 history at Kainantu. The present day strain and stress fields are characterised by ~ north-south
566 convergence in a compressional or strike-slip regime. This is compatible with the kinematics
567 of the latest faults. This tectonic setting extends back for the last 4 – 5 Ma during collision of
568 the Finisterre Terrane. The formation of the Mill, Puma and Robinson lodes and gold-copper
569 mineralization involved brecciation and dilation under a different stress regime. This occurred
570 during a change in tectonics at 9 - 6 Ma, which also lead to porphyry intrusions associated
571 with the mineralization, possibly influenced by a stalled, delaminated slab. The preceding Sm
572 and S1 formation can be related to the previous plate tectonic history of north-south
573 convergence.
574
575

We are grateful to staff of Kainantu mine, Barrick and Highlands Pacific for logistical assistance, to the reviewers for their comments and to the handling editor Peter Sorenjon-Ward.

References

Abbott, L.D., Silver, E.A., Galewsky, J. 1994. Structural evolution of a modern arc–continent collision in Papua New Guinea. Tectonics, 13, 1007–1034

Angelier, J., 1991. Analyse chronologique matricielle et succession regionale des evenments tectoniques. Comptes Rendu l'Academie Sci. Paris 312, 1633-1638.

Blenkinsop, T. G. 2006. Kinematic and dynamic fault slip analyses: implications from the surface rupture of the 1999 Chi-Chi, Taiwan, earthquake. Journal of Structural Geology, 28, 1040-1050.

Cloos, M., Sapiie, B., van Ufford, A.Q., Weiland, R.J., Warren, P.Q., & McMahon, T.P., 2005. Collisional delamination in New Guinea: the geotectonics of subducting slab breakoff. Geological Society of America, Special Paper 400.

Corbett, G.J., and Leach, T.M. 1998. Southwest Pacific Rim gold-copper systems: structure, alteration, and mineralization, short course manual, 318 p.

Corbett, G. J., T. M. Leach, M. Thirnbeck, W. Mori, T. Sione, K. Harry, K. Digan, & P. Petrie. 1994. The porphyry-related mesothermal vein gold mineralisation north of Kainantu, Papua New Guinea. In *Proceeding Volume, Papua New Guinea Geology, Exploration and Mining Conference, Lae, MP, Papua New Guinea*, pp. 113-124. 1994.

Cox, S.F., 1999. Deformational controls on the dynamics of fluid flow in mesothermal gold systems. Geological Society, London, Special Publications 155, 123–140.

Crowhurst, P.V., Hill, K. C., Foster, D.A., & Bennett, A. P. 1996. Thermochronological and geochemical constraints on the tectonic evolution of northern Papua New Guinea. In tectonic evolution of SE Asia, Ed. R. Hall & D. Blundell, Geological Society, London, Special Publications 106, 525-537.

Cullen, A. B., 1996. Ramu basin, Papua New Guinea: A record of late Miocene terrane collision. American Association of Petroleum Geologists Bulletin 80, 663-684.

Davies, H.L., and Smith, I.E. 1971. Geology of Eastern Papua. Geological Society of America Bulletin, 82, 3299-3312.

Davies, H.L., 2012. The geology of New Guinea — the cordilleran margin of the Australian

609 continent. Episodes 35, 87–102.
610 Dirks, P.H.G.M., Charlesworth, E.G., Munyai, M.R., & Wormald, R., 2013. Stress analysis,
611 post-orogenic extension and 3.01Ga gold mineralisation in the Barberton Greenstone
612 Belt, South Africa. Precambrian Research 226, 157–184.
613 Espi , J. O. , Hayashi , K. , Komuro , K. , Kajiwara , Y. & Murakami , H . 2005. The
614 Bilimoia gold deposit, Kainantu, Papua New Guinea : . In Mao , J. and Bierlein , F. P. A
615 fault-controlled, lode- type, synorogenic tellurium-rich quartz-gold vein system (eds .)
616 8th Biennial SGA Meeting , Vol. 2 ; 18 – 21 Aug 2005, Peking, China . Springer , Berlin,
617 941 – 944 .
618 Espi, J. O. Hayashi, K., Komuro., K., Kjiwara, Y., & Murakami, H. 2007. Geology, wall rock
619 alteration and vein paragenesis of the Bilimoia Gold Deposits, Kainantu Metallogenic
620 Region, Papua New Guinea. Resource Geology 57, 249-268.
621 Griffin, T.J. 1979. Granitoids of the Tertiary continent - island arc collision zone, Papua New
622 Guinea, Geological Survey Of Papua New Guinea, Report 79/22, 53p.
623 Hall, R., 2002. Cenozoic geological and plate tectonic evolution of SE Asia and the SW
624 Pacific: computer-based reconstructions, model and animations. Journal of Asian Earth
625 Sciences 20, 353–431.
626 Hamilton, W. 1979. Tectonics of the Indonesian Region United States Geological Survey
627 Professional Paper, 1078, 293–304.
628 Heidbach, O., Tingay, M., Barth, A., Reinecker, J., Kurfeß, D. & Müller, B., 2008. The World
629 Stress Map database release 2008 doi:10.1594/GFZ.WSM.Rel2008.
630 Hill, K. C. & Hall, R., 2003.Mesozoic–Cenozoic evolution of Australia's New Guinea margin
631 in a west Pacific context. In: Hillis, R.R., Müller, R.D. (Eds.), Evolution and dynamics of
632 the Australian Plate: Geological Society of Australia Special Publication 22. Geological
633 Society of America Special Paper 372, pp. 265–290.
634 Hill, K. C. & Raza, A., 1999. Arc-continent collision in Papua Guinea: Constraints from
635 fission track thermochronology. Tectonics 18, 950-966.
636 Holm, R.J., Spandler, C., & Richards, S.W., 2015. Continental collision, orogenesis and arc
637 magmatism of the Miocene Maramuni arc, Papua New Guinea. Gondwana Research 28,
638 1117–1136.
639 Hodgson, C.J., 1989. Patterns of Mineralization, in: Bursnall, J.T. (Ed.), Mineralization and
640 Shear Zones: Short Course Notes Volume 6. Montreal, pp. 51–88.
641 Klootwijk C., Giddings, J., Pigram, C., Loxton, C., Davies, H., Rogerson, R., & Falvey, D.,
642 2003a. Papua New Guinea Highlands: palaeomagnetic constraints on terrane tectonics.

643 Tectonophysics 362, 239 – 272.
644 Klootwijk, C., Giddings, J., Pigram, C., Loxton, C., Davies, H., Rogerson, R., & Falvey, D.,
645 2003b. North Sepik region of Papua New Guinea: palaeomagnetic constraints on arc
646 accretion and deformation. Tectonophysics, 362, 273–301.
647 Kreemer, C., W.E. Holt & A.J. Haines, 2003. An integrated global model of present-day plate
648 motions and plate boundary deformation, Geophysical Journal International 154, 8-34.
649 Lisle, R.J., Orife, T.O., Arlegui, L., Liesa, C. & Srivastava, D.C., 2006. Favoured states of
650 palaeostress in the Earth's crust: evidence from fault-slip data. Journal of Structural
651 Geology 28, 1051–1066.
652 Manning, C.E. & Ingebritsen, S.E., 1999. Permeability Implications of the Continental of
653 Geothermal Data Crust ' and Metamorphic Systems. Reviews of Geophysics. 37, 127–
654 150.
655 Marrett, R. & Allmendinger, R.W., 1990. Kinematic analysis of fault-slip data. Journal of
656 Structural Geology, 12, 1990, 973-986.
657 Miller, J., Blewett, R., Tunjic, J. & Connors, K., 2010. The role of early formed structures on
658 the development of the world class St Ives Goldfield, Yilgarn, WA. Precambrian
659 Research 183, 292–315.
660 Pegler, G., Das, S. & Woodhouse, J.H., 1995. A seismological study of the eastern New
661 Guinea and the western Solomon Sea regions and its tectonic implications. Geophysical
662 Journal International 122, 961–981.
663 Phillips, G.N. & Powell, R., 2009. Formation of gold deposits: Review and evaluation of the
664 continuum model. Earth-Science Reviews 94, 1–21.
665 Page, R.W. 1976. Geochronology of Igneous and Metamorphic Rocks in the New Guinea
666 Highlands. Bureau of Mineral Resources, Geology and Geophysics, Bulletin 162.
667 Poulsen, H. & Robert, F., 1989. Shear zones and gold: Practical examples from the southern
668 Canadian Shield, in: Bursnall, J.T. (Ed.), Mineralization and Shear Zones, Geological
669 Association of Canada, Short Course Notes 6. Montreal, pp. 239–266.
670 Ramsay, J.G. & Lisle, R.J., 2000. The Techniques of Modern Structural Geology. Volume 3:
671 Applications of Continuum Mechanics in Structural Geology, Academic Press, London.
672 Robert, F., Boullier, A.-M. & Firdaous, K., 1995. Gold-quartz veins in metamorphic terranes
673 and their bearing on the role of fluids in faulting. Journal of Geophysical Research: Solid
674 Earth 100, 12861–12879.

675 Sanislav, I. V., Kolling, S.L., Brayshaw, M., Cook, Y., Dirks, P.H.G.M., Blenkinsop, T.G.,
676 Mturi, M.I. & Ruhega, R., 2015. The geology of the giant Nyankanga gold deposit, Geita
677 Greenstone Belt, Tanzania. Ore Geology Reviews 69, 1–16.
678 Schellart, W.P., Lister, G.S. & Toy, V.G., 2006. A Late Cretaceous and Cenozoic
679 reconstruction of the Southwest Pacific region: Tectonics controlled by subduction and
680 slab rollback processes. Earth-Science Reviews 76, 191–233.
681 Sibson, R., 1987. Earthquake rupturing as a mineralizing agent in hydrothermal systems.
682 Geology 15, 710–704.
683 Sillitoe, R. H. 1997. Characteristics and controls of the largest porphyry copper-gold and
684 epithermal gold deposits in the circum-Pacific region, Australian Journal of Earth
685 Sciences, 44:3, 373-388, DOI: 10.1080/08120099708728318
686 Tingey , R. J. & Grainger , D. J . 1976. Markham – Papua New Guinea , 1 : 250,000
687 Geological Series with Explanatory Notes . International Index Sheet Sb/55-10 .
688 Geological Survey of Papua New Guinea , Port Moresby, 49p .
689 Tomkins, A.G. & Grundy, C., 2009. Upper temperature limits of orogenic gold deposit
690 formation: Constraints from the granulite-hosted griffins find deposit, Yilgarn craton.
691 Economic Geology 104, 669–685.
692 Tripp, G.I. & Vearncombe, J.R., 2004. Fault/fracture density and mineralization: a contouring
693 method for targeting in gold exploration. Journal of Structural Geology 26, 1087–1108.
694 Van Wyck, N. & Williams, I.S., 2002. Age and provenance of basement metasediments from
695 the Kubor and Bena Bena Blocks, central Highlands, Papua New Guinea: Constraints on
696 the tectonic evolution of the northern Australian cratonic margin. Australian Journal of
697 Earth Science 49, 565–577.
698 Vigar, A.J., Lueck, B., Taylor, I., Prendergast, K. & Dale, P. 2015. Kainantu Gold-Copper
699 System, Papua New Guinea. PACRIM 2015 Congress, Hong Kong, Australian Institute
700 of Mining and Metallurgy, Publication Series No 2/2015, 601-606.
701 Wallace, L. M., McCaffrey, R., Beavan, J. & Ellis, S. 2005: Rapid microplate rotations and
702 backarc rifting at the transition between collision and subduction. Geology11, 857–860.
703 Weiler, P.D. & Coe, R.S., 2000, Rotations in the actively colliding Finisterre-arc terrane:
704 Paleomagnetic constraints on Plio-Pleistocene evolution of the South Bismarck
705 microplate, northeastern Papua New Guinea: Tectonophysics, 316, 297–325. doi:
706 10.1016/ S0040-1951(99)00259-0.

Weinberg, R.F., Hodkiewicz, P.F. & Groves, D.I., 2004. What controls gold distribution in Archean terranes? Geology 32, 545-548.

710

711 Tables

712

713

714 Table 1. Deformation chronology at Kainantu gold mine from underground observations

715

Event	Structures	Deformation mode	Kinematics
D5	Chinook Joint	Fracture	
D4	Faults with gouge	Discontinuous deformation; faults along shear zones	N-S shortening
D3	Mill Lode style brecciation	Extension on Mill Lode: Reactivation of Sm	NE-SW extension
D2	S2 Crenulation cleavage: L_2^1 lineation, S2 Kink bands	Penetrative deformation	E-W shortening
Dm	Shear zone network Mylonites: Sm, Lm	Localized zones of dextral strike-slip; reactivation of S1	N-S to NNE-SSW shortening
D1	Regional cleavage - S1 L1 lineation, L^0_1	Penetrative deformation	N-NE shortening

716

717

718

719

720 Table 2. Sample locations (mine grid) and descriptions.

721

722

Sample	Level	E	N	Description
K1	20	29905	59771	Moderate S1, very strong S2/L_{12}
K2	20	29925	59925	Strong S1, shear zone, no Mill Lode
K3	20	29921	59956	Shear zone with Mill Lode
K4	19	28935	60040	Gouge zone
K5	19	29926	59857	Very strong S2
K6	20	29934	60031	Puma vein
K7	20	29924	60023	Mill Lode Breccia, vugs, pyrite stringers, moderate fabric
K8	20	29937	60057	Very strong foliation in shear zone
K9	20	29912	59642	Mill Lode breccia
K10	20	29903	59733	Mylonite in shear zone

723

724

725

726

727

728

729 Figure Captions

730

731 Fig. 1. Regional tectonics. Geology and intrusive ages of Maramui arc rocks supplied by
732 Barrick Gold Corporation, tectonics after Hall (2002).

733

734 Fig. 2. Geology of the area around Kainantu, showing the Kora-Irumafimpa vein system in
735 the context of other veins and intrusions. Metal zonation vectors in white arrows show
736 the distal to proximal change from Ag-(Au)-Pb-Zn to Cu-Au-Ag (Bi-Te-W) southwards.

737

738 Fig. 3. Structures exposed underground.

739 a) Strong S1 foliation in phyllites. The orientation of S1 is very consistent. Adjacent to
740 Mill Lode, 20 level.
741 b) Sigma clasts give dextral movement in mylonitic shear zone. Floor view, 20 level,
742 29905E 59758N.
743 c) L12 strongly developed. 20 level, 59770 N.
744 d) Isoclinal folds of quartz-albite vein on 20 level, 29904E, 59751N. The hinges of these
745 folds plunge parallel to L^1_2 and their axial surface is parallel to S2.
746 e) Polished surface of Mill Lode from 20 level, 59643 N, showing breccia fragments of
747 mylonite with fuchsite and open vugs linked by quartz veins. Field of view 15 cm.
748 f) Mill Lode, showing Sm cut by quartz-pyrite mineralization. Loose block from 20
749 level.
750 g) P foliation, roof view. Sinistral shear in roof view corresponds to dextral shear in map
751 view. 19 level, Mill drive North.
752 h) Asymmetric boudins, Riedel shear & P foliation indicating sinistral shear in roof view
753 corresponding to dextral shear in map view.19 Level, Mill Drive North.

754

755 Fig. 4. Stereoplots of structural data from levels 17 to 21. All plots are lower hemisphere,
756 equal area. Symbols identified in key. KB = Kink band, KPAP = Kink band axial plane.
757 The main features on each level are broadly similar: S1/Sm strikes NW-SE and dips
758 steeply, L1/Lm is subhorizontal, and L^1_2 and kink band hinges plunge moderately SE.
759 The dispersion of S1/Sm poles on level 20 partly reflects the northern end of the level
760 where there is a marked obliquity between the foliations and the general trend of the
761 shear zones and foliations.

762

763 Fig. 5. Mapping on 20 level, Kainantu mine. The lower part of each panel connects to the top
764 of the one to the right. Shear zones in bright yellow are notably parallel to S1
765 measurements except at the northern end where a significant obliquity corresponds to
766 higher grades; this is probably due to D2 folding . Lodes occur with shear zones. Faults
767 (blue) are also parallel to the shear zone network, which has a geometry of NW longer,
768 NW striking segments joined by shorter NNW segments. L1 and Lm are sub-horizontal
769 within the NW striking S1/Sm. L^1_2 plunges SE, parallel to kink bands, and to bends in the
770 shear zone network. Coordinates are in metres on the mine grid.
771
772 Fig. 6. Microstructures.
773 a) Sm defined by quartz/phyllosilicate banding and phyllosilicate grain shape fabric. In
774 this high strain sample, quartz grain shapes also contribute to the fabric. Sample K10,
775 crossed polars, 2 mm. In all figure captions. plane polarised light.
776 b) Sm mylonitic fabric created by folding and crenulation of S1 fabric. K8, plane
777 polarised light.
778 c) S2 defined by asymmetric crenulation cleavage of S1. A band of S1 quartz can be
779 seen deformed by S2 on the centre-upper right of the picture. K1, crossed polars.
780 d) Vq with typical fibrous to blocky filling cuts Sm but is deformed into Sm where it
781 becomes parallel to the lower edge of the picture. Quartz near lower edge may be a
782 deformed Vq vein. K7, crossed polars.
783 e) Vq (vertical) is cut by Vqp (horizontal) K6, plane polarised light.
784 f) Breccia, K6, plane polarised light.
785
786 Fig. 7. Younging Table. Younging table for relationships of veins and structures. The table is
787 read from the row headings on the right hand side across to the column headings at the
788 top. Numbers indicate an “is older than” relationship. For example, there is one
789 observation that Vqp is older than Vc.
790
791 Fig. 8. Microstructural history integrating fabrics and microstructures, mineral and vein
792 paragenesis.
793
794 Fig. 9. Equal area lower hemisphere stereoplots of fault plane orientations. a) Poles to all 76
795 fault planes and 34 slickenlines. b) Great circles and slickenlines to 14 faults with slip senses.
796 Arrows show direction of hangingwall movement. c) Kinematic analysis showing maximum,

intermediate and least principal strain axes (1, 2, 3). Shortening (3) is NS. d) Dynamic analysis by the right trihedra method: σ_1 is North-South. e) Dynamic analysis by inversion. σ_1 is North-South and σ_2 is subvertical. The stress ratio Φ , $(\sigma_2 - \sigma_3)/(\sigma_1 - \sigma_3)$, is 0.3.

Fig. 10. Long Section, looking SW between the Kora and Irumafimpa ends of the Kora-Irumafimpa veins system. Ore shoots, defined by gold grades indicated on the section, plunge SE, parallel to L^1_2 and to bends in the shear zone network.

Fig. 11. Synthesis of tectonics of NE Papua New Guinea for the last 20 Ma, based on references shown. Scales on sides in Ma. MaB – Manus basin, WoB – Woodlark Basin, NBT – New Britain Trench, SCT – San Cristobal Trench.

Fig. 12. Present day strain rates in Papua New Guinea relative to Australia. The black arrows indicate NE convergence of PNG with Australia. The white arrows indicate extension. Colours show the second invariant of the strain rate tensor; red colours to the north of Papua New Guinea indicate the largest strain rates i.e. the plate boundary, but significant strain rates occur in the eastern Highlands. Source: ILP Global strain rate map, Kreemer et al., (2003). http://jules.unavco.org/Voyager/ILP_GSRM?e=144.147942157954&n=-5.11375899068257&de=3.60201599406836&dn=3.2116455312831&gmt=4&vel=512

Fig. 13. Present day stress field in Papua New Guinea. Lines give direction of largest horizontal stress. Abbreviations in key: NF – Normal fault regime, SS – Strike slip fault regime, TF – Thrust fault regime (Source: World Stress Map, 2008: Heidbach et al. 2008).

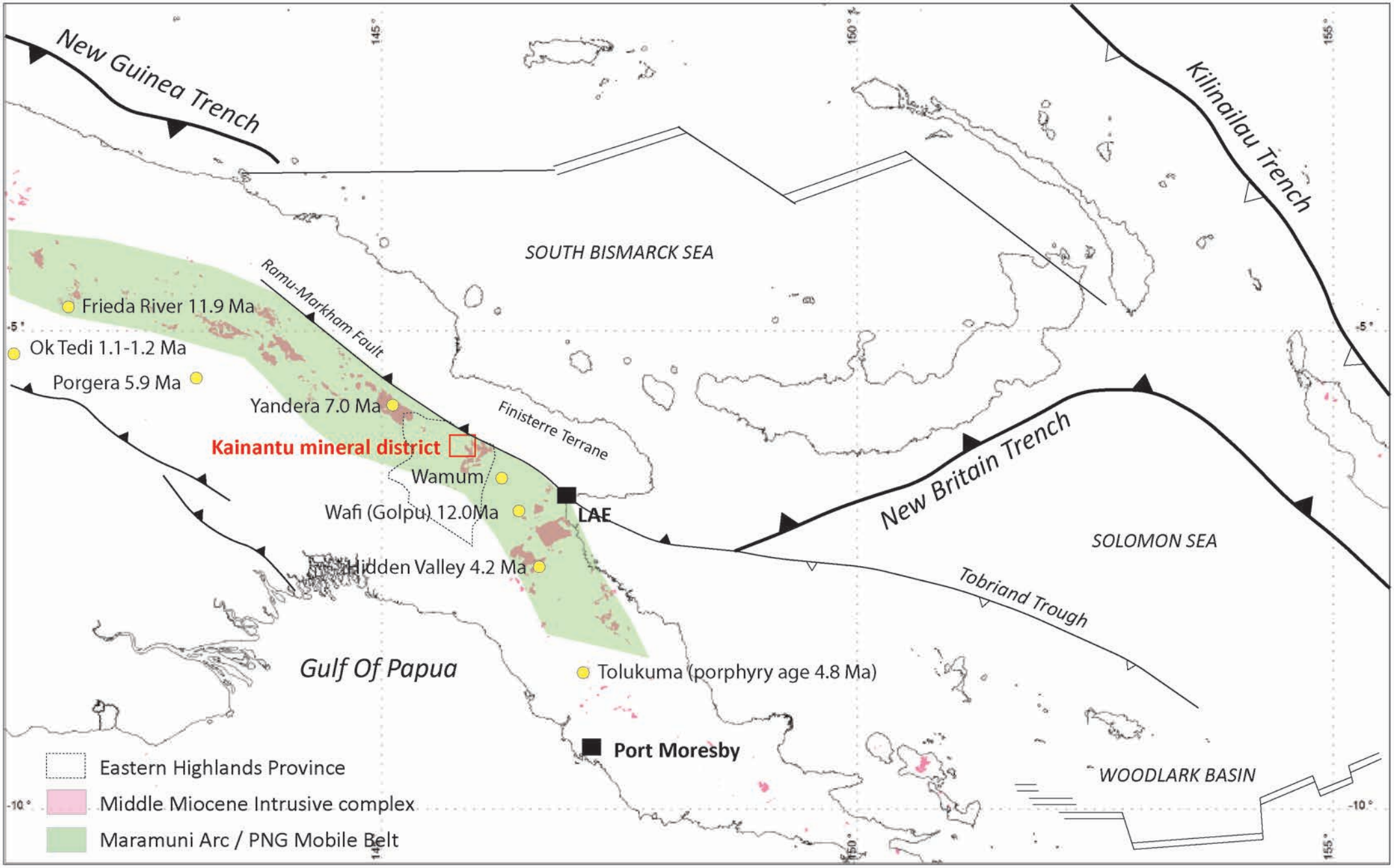
New Guinea Trench
Kilinailau Trench
SOUTH BISMARCK SEA
Ramu-Markham Fault
Frieda River 11.9 Ma
Ok Tedi 1.1-1.2 Ma
Porgera 5.9 Ma
Yandera 7.0 Ma
Finisterre Terrane
Kainantu mineral district
Wamum
Wafi (Golpu) 12.0Ma
LAE
New Britain Trench
SOLOMON SEA
Hidden Valley 4.2 Ma
Tobriand Trough
Gulf Of Papua
Tolukuma (porphyry age 4.8 Ma)
Port Moresby
WOODLARK BASIN
Eastern Highlands Province
Middle Miocene Intrusive complex
Maramuni Arc / PNG Mobile Belt
145°
150°
155°
-5°
-10°

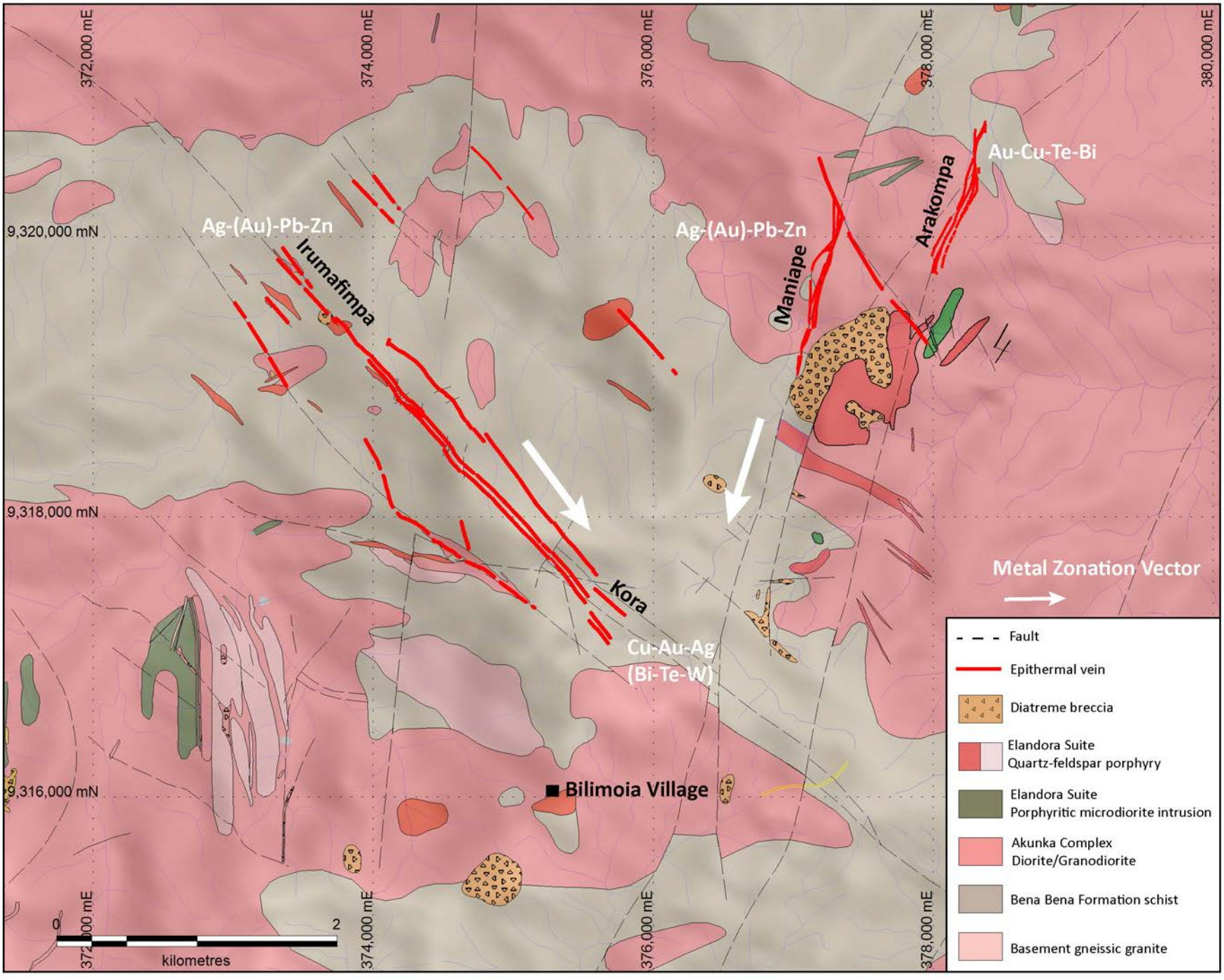
372,000 mE
374,000 mE
376,000 mE
378,000 mE
380,000 mE
9,320,000 mN
9,318,000 mN
9,316,000 mN
Ag-(Au)-Pb-Zn
Irumafimpa
Ag-(Au)-Pb-Zn
Maniape
Arakompa
Au-Cu-Te-Bi
Kora
Cu-Au-Ag
(Bi-Te-W)
Metal Zonation Vector
Bilimoia Village
0
2
kilometres
Fault
Epithermal vein
Diatreme breccia
Elandora Suite
Quartz-feldspar porphyry
Elandora Suite
Porphyritic microdiorite intrusion
Akunka Complex
Diorite/Granodiorite
Bena Bena Formation schist
Basement gneissic granite

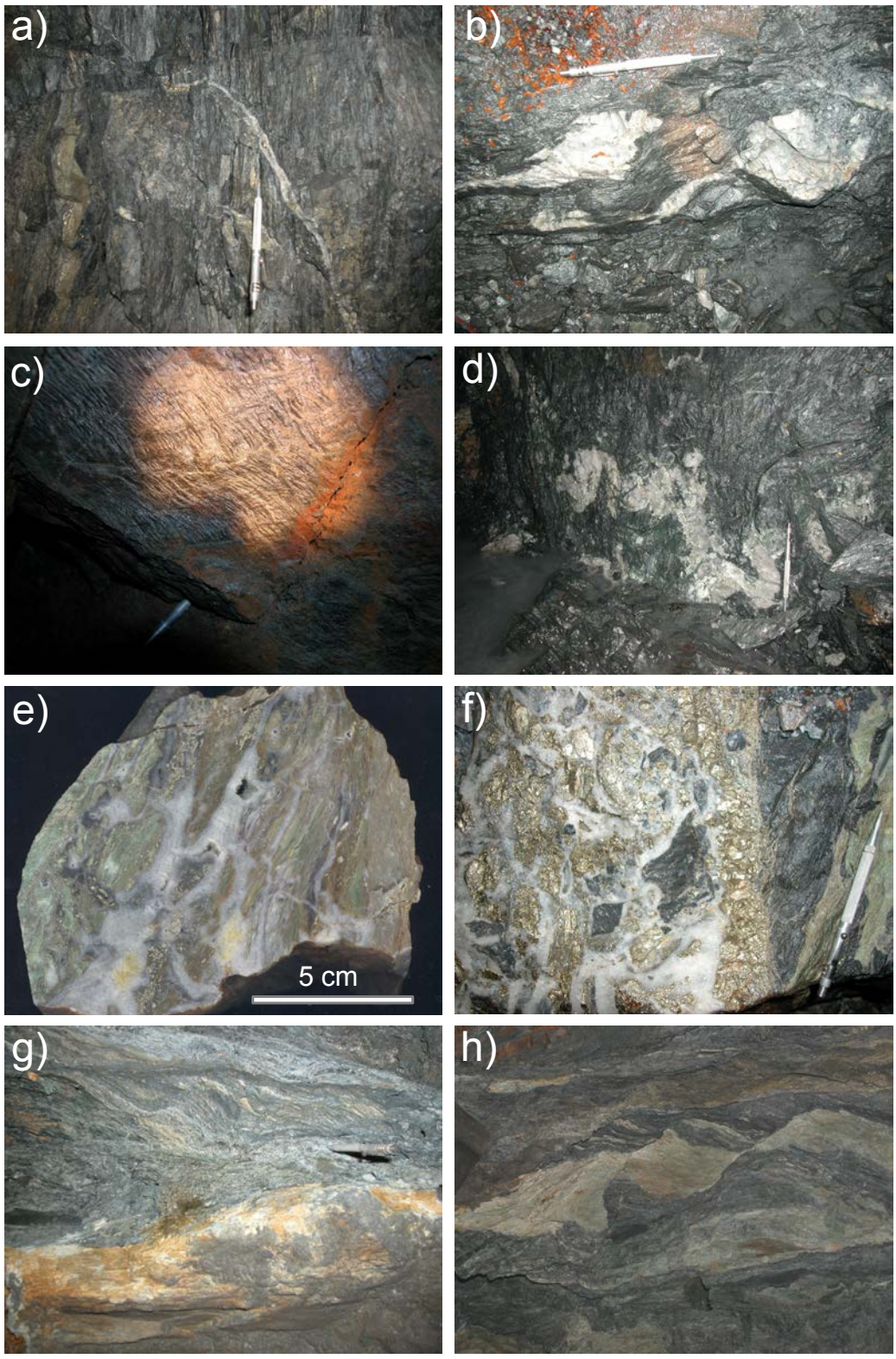
a)
b)
c)
d)
e)
5 cm
f)
g)
h)

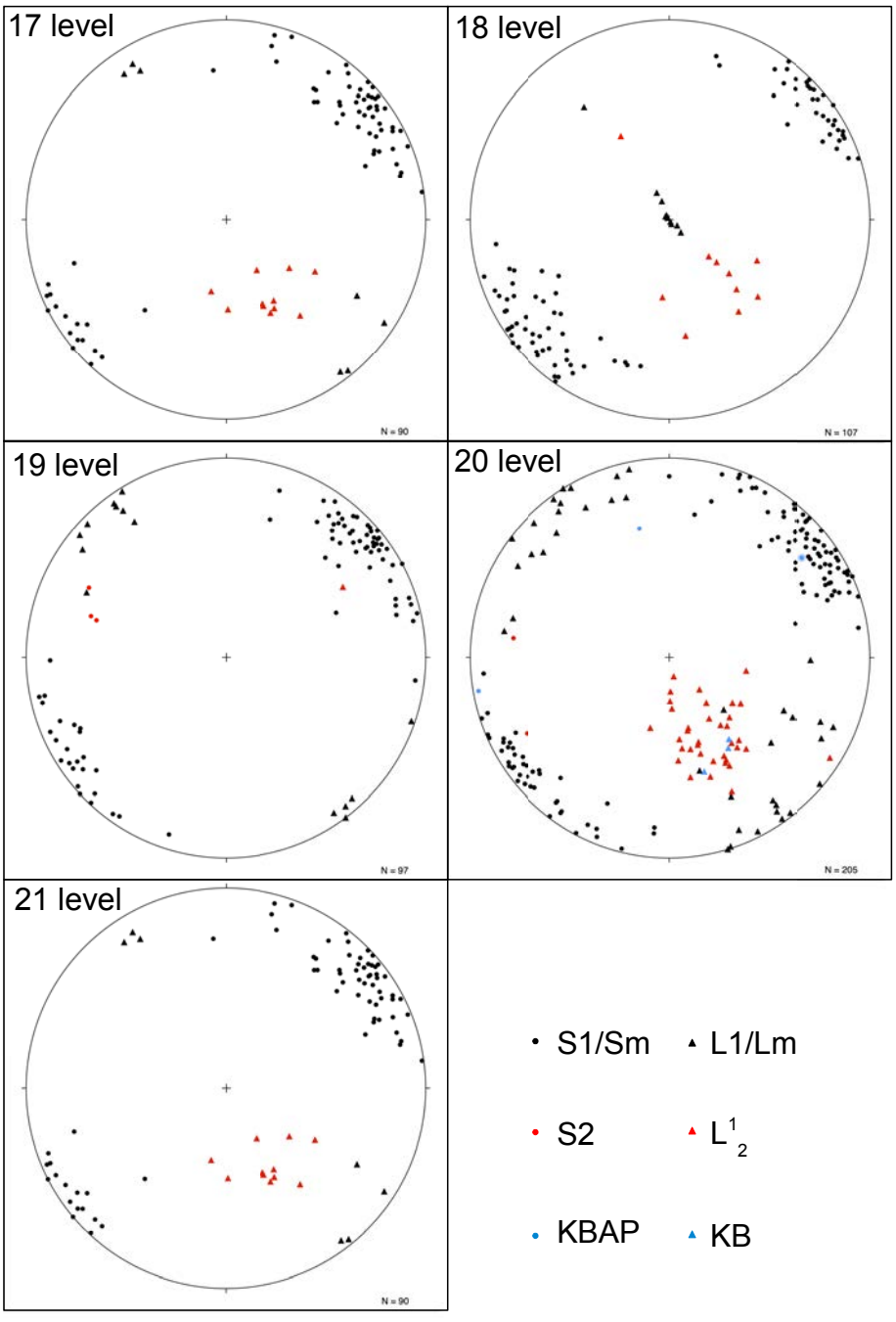
17 level
N = 90
18 level
N = 107
19 level
N = 97
20 level
N = 205
21 level
N = 90
S1/Sm
L1/Lm
S2
L 1 2
KBAP
KB

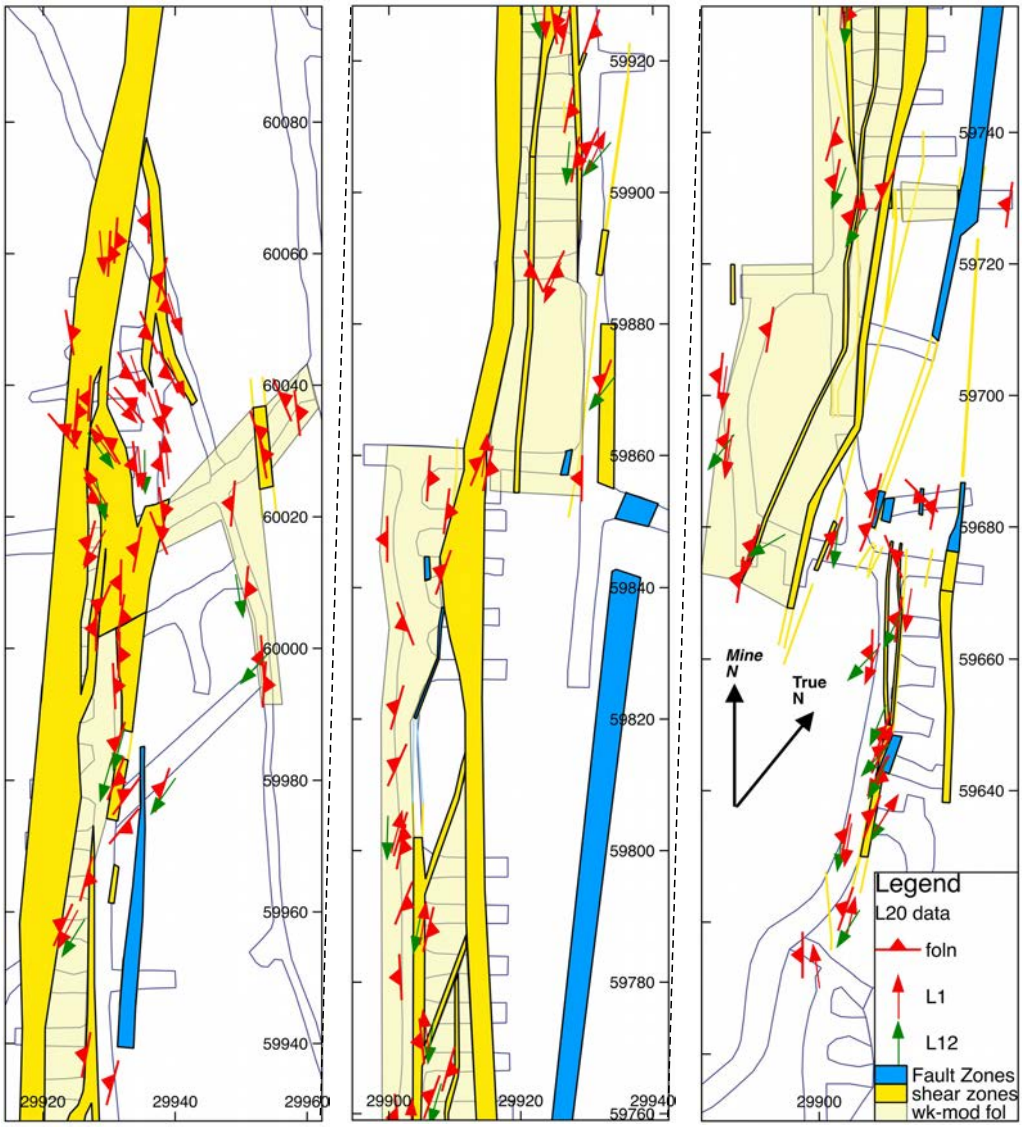
60080
60060
60040
60020
60000
59980
59960
59940
29920
29940
29960
59920
59900
59880
59860
59840
59820
59800
59780
59760
29900
29920
29940
59740
59720
59700
59680
59660
59640
29900
Mine N
True N
Legend
L20 data
foln
L1
L12
Fault Zones
shear zones
wk-mod fol

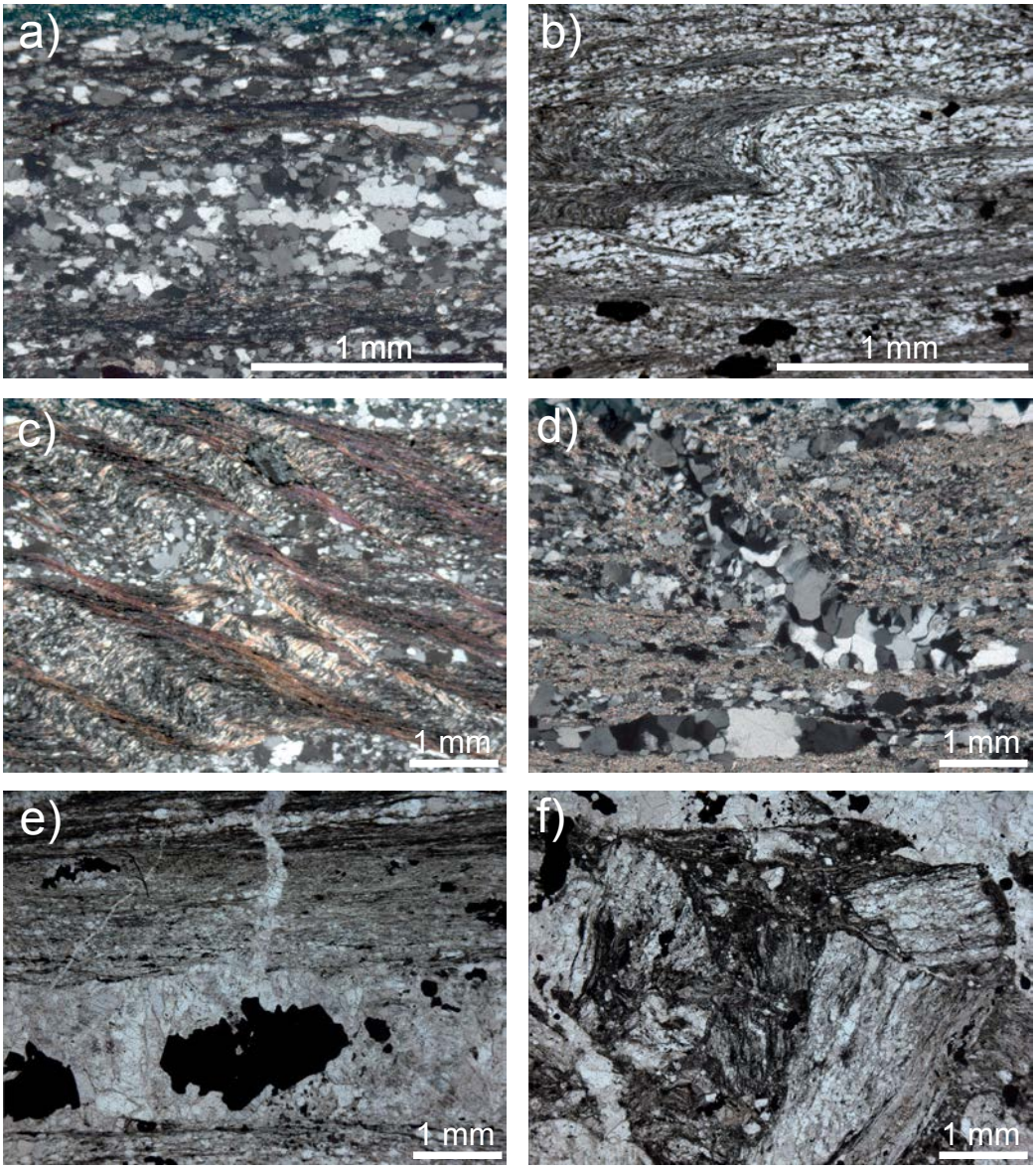
a)
1 mm
b)
1 mm
c)
1 mm
d)
1 mm
e)
1 mm
f)
1 mm

	Sm	Vq	S2	Vqp	Vqc	Vsp	Vc	Vt
Sm		1	1	1	1	1	1	1
Vq			1	1		1		
S2								
Vqp							1	
Vqc								
Vsp								
Vc								1
Vt								

Event	Fabrics & microstructures	Mineral Paragenesis	Vein Paragenesis
		garnet muscovite chlorite sericite	Vq Vqp Vqc Vsp Vc Vt
D4 Faulting	P foliation and R shears		
D3 Brecciation in Lodes	Breccia veins; vugs; pallisade textures		
D2 S2 Crenulation	Asymmetric crenulation cleavage; kink bands		
Dm Mylonites	Mylonitic fabric: quartz recrystallisation grain boundary migration grain boundary pinning ribbon quartz		
D1 Regional cleavage	S1 cleavage defined by muscovite		

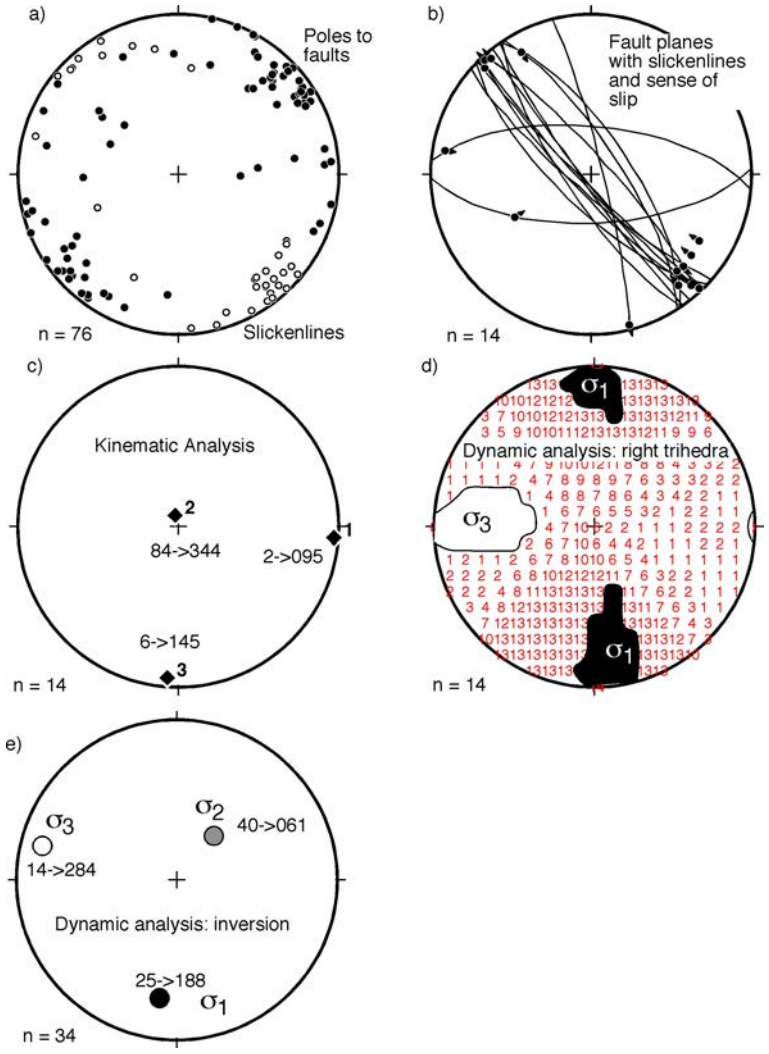
a)
Poles to faults
n = 76
Slickenlines
b)
Fault planes with slickenlines and sense of slip
n = 14
c)
Kinematic Analysis
2
84->344
1
2->095
6->145
3
n = 14
d)
σ1
Dynamic analysis: right trihedra
σ3
σ1
n = 14
e)
σ3
14->284
σ2
40->061
Dynamic analysis: inversion
25->188
σ1
n = 34

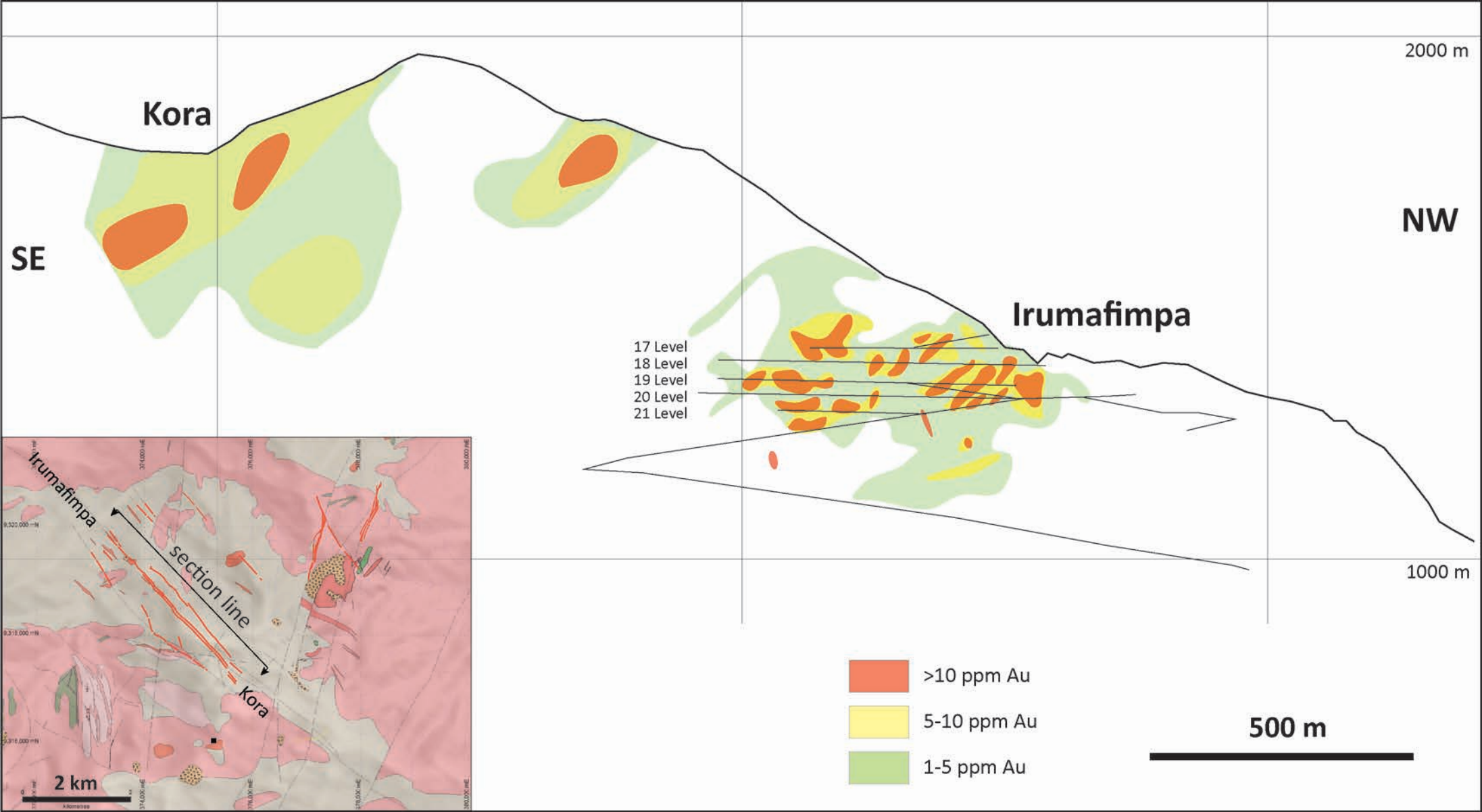
2000 m
Kora
SE
NW
Irumafimpa
17 Level
18 Level
19 Level
20 Level
21 Level
1000 m
Irumafimpa
section line
Kora
2 km
>10 ppm Au
5-10 ppm Au
1-5 ppm Au
500 m

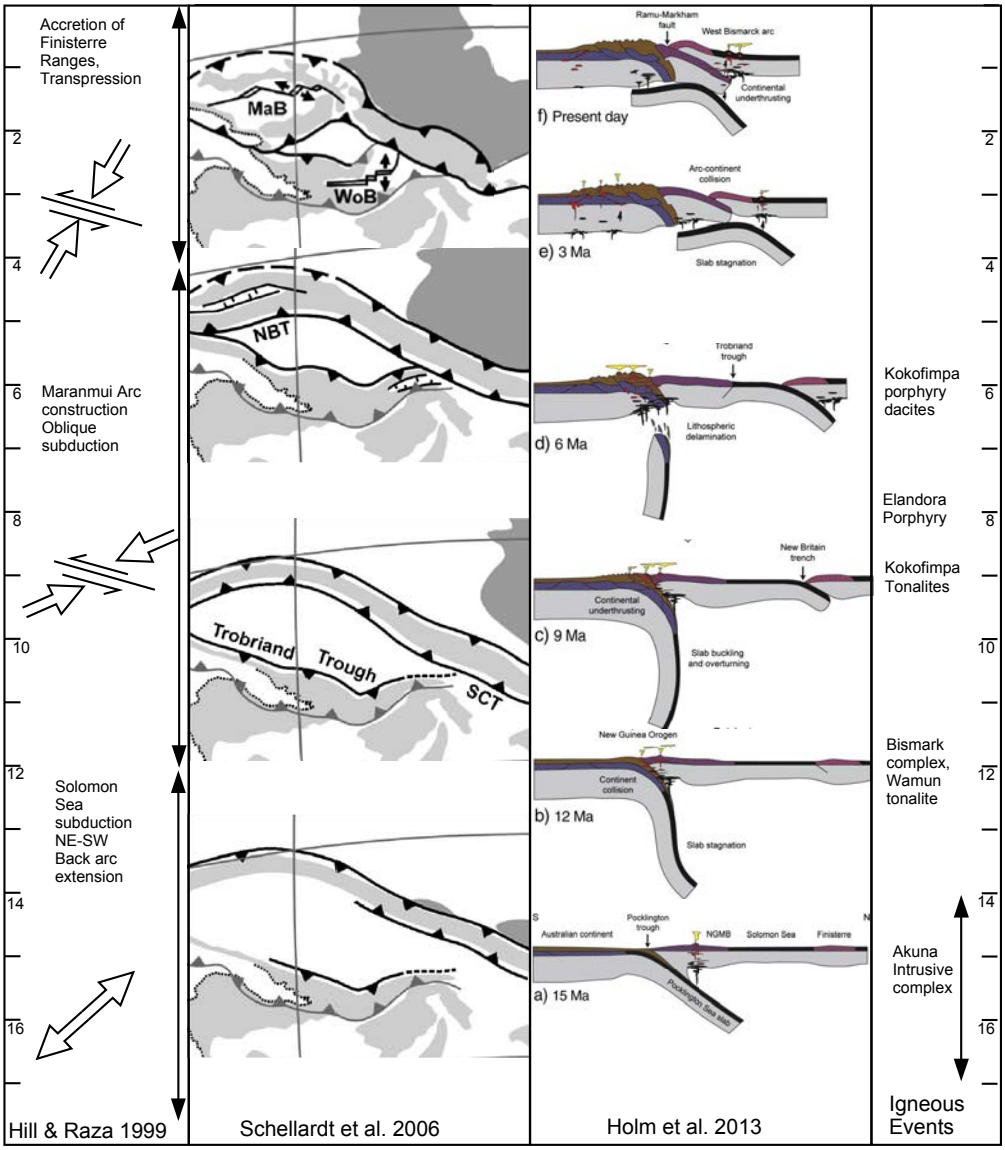
Accretion of Finisterre Ranges, Transpression
Maranmui Arc construction Oblique subduction
Solomon Sea subduction NE-SW Back arc extension
2
4
6
8
10
12
14
16
MaB
WoB
NBT
Trobriand
Trough
SCT
Ramu-Markham fault
West Bismarck arc
Continental underthrusting
f) Present day
Arc-continent collision
e) 3 Ma
Slab stagnation
Trobriand trough
Lithospheric delamination
d) 6 Ma
New Britain trench
Continental underthrusting
c) 9 Ma
Slab buckling and overturning
New Guinea Orogen
Continent collision
b) 12 Ma
Slab stagnation
S
Australian continent
Pocklington trough
NGMB
Solomon Sea
Finisterre
N
a) 15 Ma
Pocklington Sea slab
Kokofimpa porphyry dacites
Elandora Porphyry
Kokofimpa Tonalites
Bismark complex, Wamun tonalite
Akuna Intrusive complex
Hill & Raza 1999
Schellardt et al. 2006
Holm et al. 2013
Igneous Events

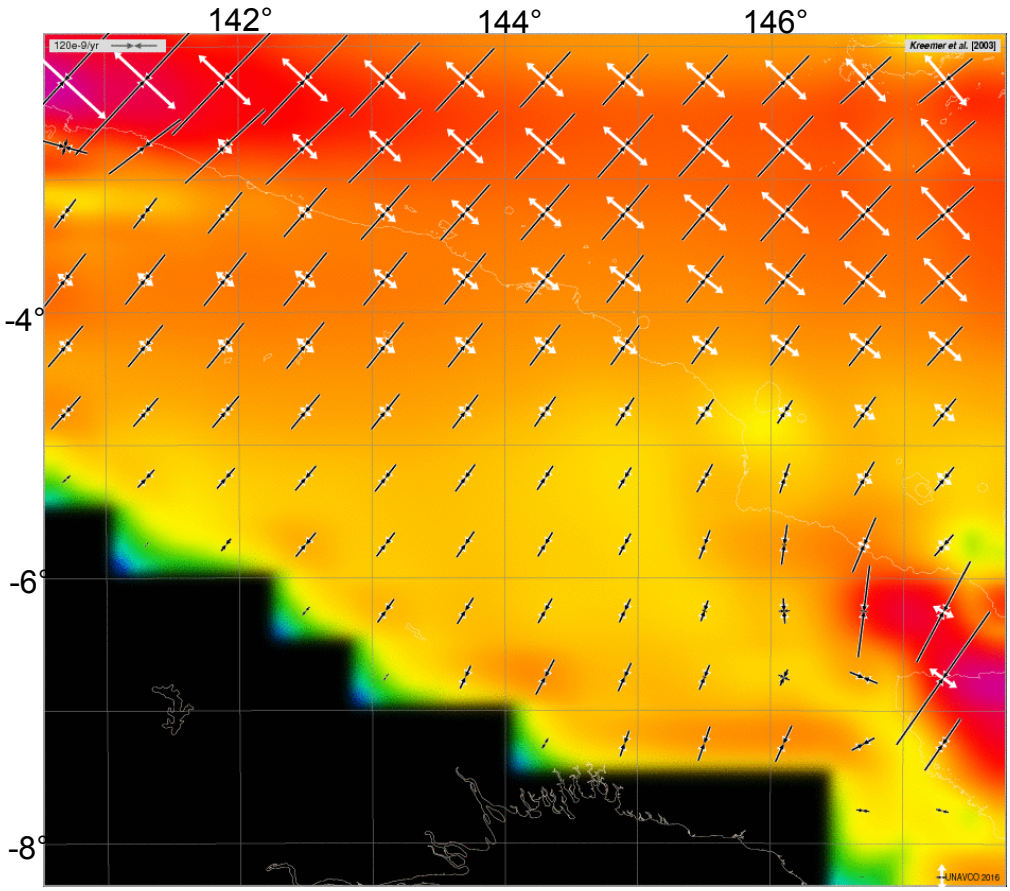
142°
144°
146°
-4°
-6°
-8°
120e-9/yr
Kreemer et al. [2003]
UNAVCO 2016

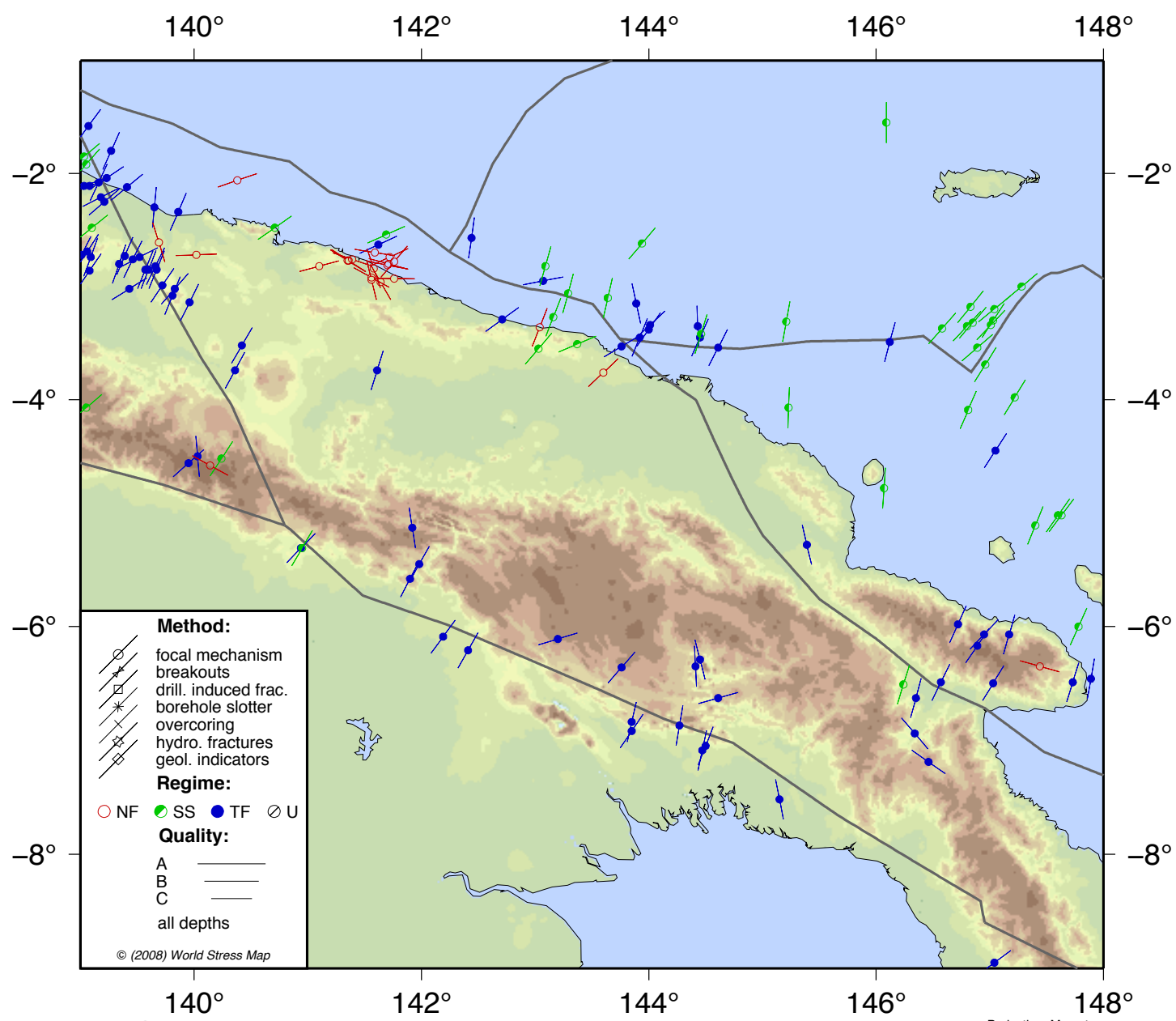
140°
142°
144°
146°
148°
−2°
−4°
−6°
−8°
Method:
focal mechanism
breakouts
drill. induced frac.
borehole slotter
overcoring
hydro. fractures
geol. indicators
Regime:
NF
SS
TF
U
Quality:
A
B
C
all depths
© (2008) World Stress Map